Available online at www.sciencedirect.com
SCIENCE DIRECT®
Journal of Solid State Chemistry 175 (2003) 231–236
JOURNAL OF SOLID STATE CHEMISTRY
http://elsevier.com/locate/jssc

Platinum silicon antimonide (PtSiSb)

Meitian Wang, Mark G. Morgan, and Arthur Mar*

Department of Chemistry, University of Alberta, Edmonton, AB, Canada T6G 2G2

Received 10 January 2003; received in revised form 25 April 2003; accepted 6 May 2003

Abstract

Platinum silicon antimonide (PtSiSb) was obtained as a byproduct of a reaction of Pt and Sb in a silica tube. Its structure was determined from X-ray diffraction data (orthorhombic, space group *Pbca*, $Z = 8$, $a = 6.3128(8)$ Å, $b = 6.3347(8)$ Å, $c = 11.3945(12)$ Å). PtSiSb is closely related to PtSiTe, which adopts a ternary ordered pararammelsbergite (α-$NiAs_2$)-type structure. The structure of PtSiSb consists of a three-dimensional network built up by condensing $PtSi_3Sb_3$ octahedra through both corner- and edge-sharing. As in all representatives of the parent α-$NiAs_2$-type structure, anion–anion pairs are present in PtSiSb. However, the electron count in PtSiSb is $19e^-$ per formula unit, one electron less than that for α-$NiAs_2$-type structures. This oxidation results in a significant distortion in the PtSiSb structure related to the occurrence of metal–metal pairs. Extended Hückel calculations were carried out on PtSiSb and PtSiTe to analyze these structural transformations as a function of electron count. A narrow band gap (< 1 eV) is predicted for PtSiSb; experimental measurements revealed that the resistivity is high ($\rho_{300} = 0.2\,\Omega$ cm) and weakly temperature dependent, suggesting a small degree of nonstoichiometry or impurity.

Keywords: Antimony; Platinum; Silicon; Crystal structure; Band structure

1. Introduction

Among ternary nickel-group silicon pnictides *M*–Si–*Pn* (*M* = Ni, Pd, Pt; *Pn* = P, As, Sb, Bi), the only known examples to date are Ni_2SiP [1], $NiSi_3P_4$ [2], $Ni_5Si_2P_3$ [3], $NiSi_2P_3$ [4] (previously misidentified as "$Ni_{3.36}Si_{1.76}P_6$" [5]), $Ni_7Si_2P_5$ [6], Ni_2SiAs [7], $PtSi_3P_2$ [8], and $PtSi_2P_2$ [8]. This survey exemplifies the relative paucity of ternary pnictides involving the heavier congeners. As well, the structures of the Ni–Si–P phases are subject to crystallographic difficulties in distinguishing between Si and P atoms [4].

Reported here is the equiatomic compound platinum silicon antimonide (PtSiSb), the first phase found in the Pt–Si–Sb system. Both metal–metal and nonmetal–nonmetal bonding are implicated in its structure, which is a distorted variant of that of PtSiTe [9]. The influence of electron count on the structure of PtSiSb was investigated through extended Hückel band structure calculations, and a resistivity measurement was carried out to test the expectation that PtSiSb should have a band gap.

*Corresponding author. Fax: +780-492-8231.
E-mail address: arthur.mar@ualberta.ca (A. Mar).

2. Experimental

2.1. Synthesis

In the course of investigating the ternary Hf–Pt–Sb system, a mixture of Hf, Pt, and $HfSb_2$ in a 1:2:1 ratio on a 0.25-g scale was arc-melted in a Centorr 5TA tri-arc furnace under argon. The product was annealed in the presence of 0.054 g HfI_4 in an evacuated fused-silica tube placed in two-zone furnace with a temperature gradient of 850/900°C for 2 days, and then cooled to room temperature over 1 day. A few irregular block-shaped crystals were isolated and were found to contain Pt, Si, and Sb in the ratio 1:1:1 (33(2)% Pt, 34(2)% Si, 33(2)% Sb) from an energy-dispersive X-ray (EDX) analysis on a Hitachi S-2700 scanning electron microscope. Evidently, the silica tube served as the source of Si in these crystals. Subsequent attempts to prepare this compound by arc-melting the elemental components resulted only in mixtures of binary silicides and antimonides. Direct reaction of Pt, Si, and Sb in a 1:1:1 ratio in a silica tube at 600°C for 1 day and 1000°C for 3 days yields a mixture of $PtSb_2$ and PtSi, which are particularly stable competing phases, as well as PtSiSb (35(2)% Pt, 32(2)% Si, 33(2)% Sb by EDX analysis).

0022-4596/03/$ - see front matter © 2003 Elsevier Inc. All rights reserved.
doi:10.1016/S0022-4596(03)00252-4

The difficulty in preparing PtSiSb may be related to the assertion that α-$NiAs_2$-type compounds represent low-temperature phases that undergo very sluggish transformations to marcasite-type phases [10]. The possibility of impurity stabilization cannot be ruled out, although the structure is quite dense and it is not obvious where interstitial defects might enter. Further phase analysis of this and related systems is in progress.

2.2. Structure determination

After the selected crystal was confirmed to be single by Weissenberg photography, intensity data were collected on an Enraf-Nonius CAD4 diffractometer at 22°C. Crystal data and further details of the data collection are given in Table 1. All calculations were carried out with use of the SHELXTL (version 5.1) package [11]. Conventional atomic scattering factors and anomalous dispersion corrections were used [12]. Intensity data were processed, and face-indexed numerical absorption corrections were applied in XPREP. The systematic absences ($0\,k\,l,\ k=2n+1;\ h\,0\,l,\ l=2n+1;\ h\,k\,0,\ h=2n+1$) are consistent uniquely with the centrosymmetric space group *Pbca*. Initial positions for all atoms were located by direct methods. Refinements proceeded in a straightforward manner and revealed no evidence for partial occupancy of sites (refined occupancies were 1.00(7) for Pt, 0.99(7) for Si, and 0.99(7) for Sb). The final difference electron density map is featureless. The atomic positions of PtSiSb were standardized with the program STRUCTURE TIDY [13]. Final values of the positional and displacement parameters are given in Table 2. Interatomic distances are listed in Table 3. Further data, in the form of a CIF, have been sent to Fachinformationszentrum Karlsruhe, Abt. PROKA, 76344 Eggenstein-Leopoldshafen, Germany, as supplementary material No. CSD-413194 and can be obtained by contacting FIZ (quoting the article details and the corresponding CSD numbers).

Table 1
Crystallographic data for PtSiSb

Formula	PtSiSb
Formula mass (amu)	344.93
Space group	D_{2h}^{15} –*Pbca* (No. 61)
a (Å)[a]	6.3128(8)
b (Å)[a]	6.3347(8)
c (Å)[a]	11.3945(12)
V (Å^3)	455.66(9)
Z	8
ρ_{calcd} (g cm^{-3})	10.056
Crystal dimensions (mm)	0.06 × 0.05 × 0.04
Radiation	Graphite monochromated Mo*K*α, λ = 0.71073 Å
μ(Mo*K*α) (cm^{-1})	732.65
Transmission factors	0.057–0.136
2θ limits	7.16° ⩽ 2θ (Mo*K*α) ⩽ 69.92°
Data collected	$-10\leqslant h\leqslant 10$, $-10\leqslant k\leqslant 10$, $-18\leqslant l\leqslant 18$
No. of data collected	7204
No. of unique data, including $F_o^2<0$	997
No. of unique data, with $F_o^2>2\sigma(F_o^2)$	854
No. of variables	29
$R(F)$ for $F_o^2>2\sigma(F_o^2)$[b]	0.042
$R_w(F_o^2)$[c]	0.098
Goodness of fit	1.097
$(\Delta\rho)_{max}$, $(\Delta\rho)_{min}$ (e Å^{-3})	3.88, −3.87

[a] Obtained from a refinement constrained so that $\alpha=\beta=\gamma=90°$.
[b] $R(F)=\sum||F_o|-|F_c||/\sum|F_o|$.
[c] $R_w(F_o^2)=[\sum[w(F_o^2-F_c^2)^2]/\sum wF_o^4]^{1/2}$; $w^{-1}=[\sigma^2(F_o^2)+(0.0432p)^2+13.5847p]$ where $p=[\max(F_o^2,0)+2F_c^2]/3$.

Table 2
Atomic coordinates and equivalent isotropic displacement parameters for PtSiSb

Atom	Wyckoff position	*x*	*y*	*z*	U_{eq} (Å^2)[a]
Pt	8*c*	0.00952(6)	0.11584(6)	0.10741(3)	0.0048(2)
Si	8*c*	0.3546(5)	0.2616(5)	0.0752(3)	0.0062(5)
Sb	8*c*	0.11706(11)	0.00222(12)	0.32746(6)	0.0062(2)

[a] U_{eq} is defined as one-third of the trace of the orthogonalized U_{ij} tensor.

Table 3
Comparison of distances (Å) and Mulliken overlap populations in PtSi*X* (*X* = Sb, Te)[a]

	PtSiSb		PtSiTe	
	Distance	MOP	Distance[b]	MOP
Pt–Si	2.395(3)		2.405(3)	
Pt–Si^{i}	2.426(3)	0.452	2.379(3)	0.485
Pt–Si^{ii}	2.430(3)		2.391(3)	
Pt–*X*^{iii}	2.6796(9)		2.701(1)	
Pt–*X*^{iv}	2.6845(8)	0.496	2.672(1)	0.470
Pt–*X*	2.6955(8)		2.737(1)	
Pt–Pt^{v}	2.8565(8)	0.093	3.698(2)	−0.103
Si–*X*^{vi}	2.584(3)	0.686	2.576(3)	0.581

[a] Symmetry codes: (i) $x-\frac{1}{2},\frac{1}{2}-y,-z$; (ii) $\frac{1}{2}-x,y-\frac{1}{2},z$; (iii) $-x,\frac{1}{2}+y,\frac{1}{2}-z$; (iv) $x-\frac{1}{2},y,\frac{1}{2}-z$; (v) $-x,-y,-z$; (vi) $\frac{1}{2}+x,y,\frac{1}{2}-z$.
[b] Ref. [9].

2.3. Electrical resistivity

Single crystals typically less than 0.2 mm in their longest dimension were mounted in a two-probe configuration for ac resistivity measurements between 2 and 300 K on a Quantum Design PPMS system equipped with an ac-transport controller (Model 7100). A current of 0.1 mA and a frequency of 16 Hz were used.

2.4. Band structure

Tight-binding extended Hückel band structure calculations on PtSiSb and PtSiTe were performed with use of the EHMACC suite of programs [14,15]. The atomic parameters were taken from literature values [16] and are listed in Table 4. Properties were extracted from the band structure using 256 k points in the irreducible portion of the Brillouin zone.

3. Results and discussion

3.1. Structure

PtSiSb is the first antimonide found in the (Ni, Pd, Pt)–Si–(P, As, Sb, Bi) systems, in which only eight phases were previously known. Fig. 1 shows the structure of PtSiSb portrayed in different ways. Each Pt atom is coordinated by three Si and three Sb atoms in an octahedral fashion. The Pt–Si distances of 2.395(3)–2.430(3) Å are somewhat shorter than those in PtSi (2.407(7)–2.638(5) Å) [17], and the Pt–Sb distances of 2.6796(9)–2.6955(8) Å are somewhat longer than that in $PtSb_2$ (2.671(2) Å) [18]. Two $[PtSi_3Sb_3]$ octahedra share an Si–Si edge to form a $[Pt_2Si_4Sb_6]$ dimer with a Pt–Pt separation of 2.8565(8) Å. This distance is somewhat longer than the 2.774 Å distance found in elemental Pt [19], but whether it is to be interpreted as a metal–metal bond will be discussed later. The $[Pt_2Si_4Sb_6]$ dimers then share all corners with each other to form a three-dimensional network, as shown in Fig. 1a. The anions form pairs with Si–Sb bond distances of 2.584(3) Å, which is nearly identical to the sum of the Pauling single bond radii of Si and Sb ($r_{Si} + r_{Sb} = 1.173 + 1.41 = 2.583$ Å) [20], so an Si–Sb single bond can be assumed. In addition to the bonded nonmetal atom, each anion (Si and Sb) is surrounded by three Pt atoms resulting in a distorted tetrahedral coordination.

The structure of PtSiSb can be derived from that of α-$NiAs_2$, also called by its mineral name pararammelsbergite, a relatively uncommon type [21,22]. Both have the same space group and a similar atomic arrangement (*Pbca*; Pearson symbol *oP*24). Anion–anion pairs occur in both structures (Si–Sb vs. As–As). PtSiSb can therefore be regarded as a ternary ordered variant of α-$NiAs_2$, which is an intermediate between the pyrite and marcasite structures. Fig. 1b and c show that the stacking of layers of octahedra along the c-axis alternates between pyrite- and marcasite-type blocks. In pyrite, the anion–anion pairs change orientation from one layer to the next, whereas in marcasite, they remain in the same disposition, as shown in Fig. 1b. A more conventional description is that the octahedra share only corners in pyrite whereas they share both corners and edges in marcasite, as shown in Fig. 1c. This polyhedral representation also reveals that the centers of the $[Pt_2Si_4Sb_6]$ fused octahedral dimers are in an fcc-type arrangement elongated along c.

Table 4
Extended Hückel parameters

Atom	Orbital	H_{ii} (eV)	ζ_{i1}	c_1	ζ_{i2}	c_2
Pt	6*s*	−7.08	2.51			
	6*p*	−5.48	1.84			
	5*d*	−12.6	4.851	0.6314	2.588	0.5288
Si	3*s*	−14.7	1.634			
	3*p*	−8.08	1.428			
Sb	5*s*	−18.8	2.323			
	5*p*	−11.7	1.999			
Te	5*s*	−20.78	2.51			
	5*p*	−13.20	2.16			

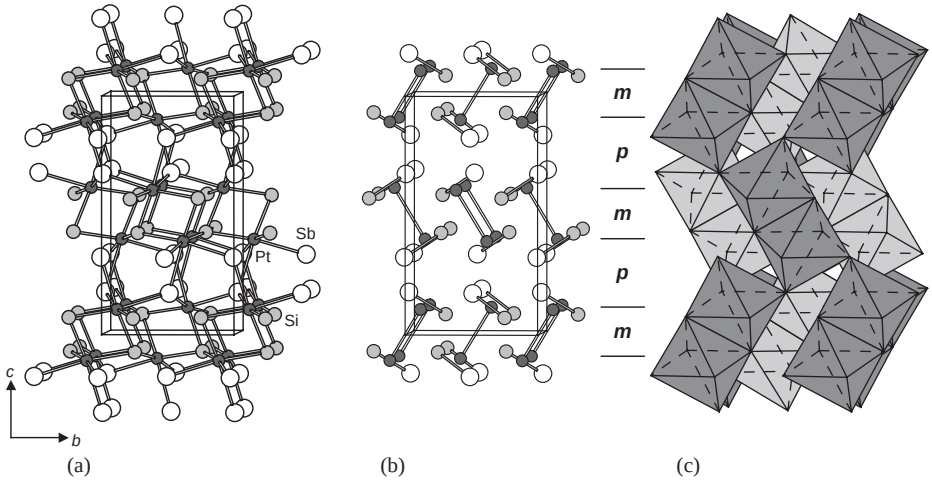

Fig. 1. Views of PtSiSb down the a-axis. In (a) and (b), the small solid circles are Pt atoms, the medium lightly shaded circles are Si atoms, and the large open circles are Sb atoms. The arrangement of Si–Sb and Pt–Pt pairs is emphasized in (b), whereas a polyhedral representation showing the connectivity of $[PtSi_3Sb_3]$ octahedra is emphasized in (c). Pyrite- (***p***) and marcasite-type (***m***) blocks alternate along the c direction.

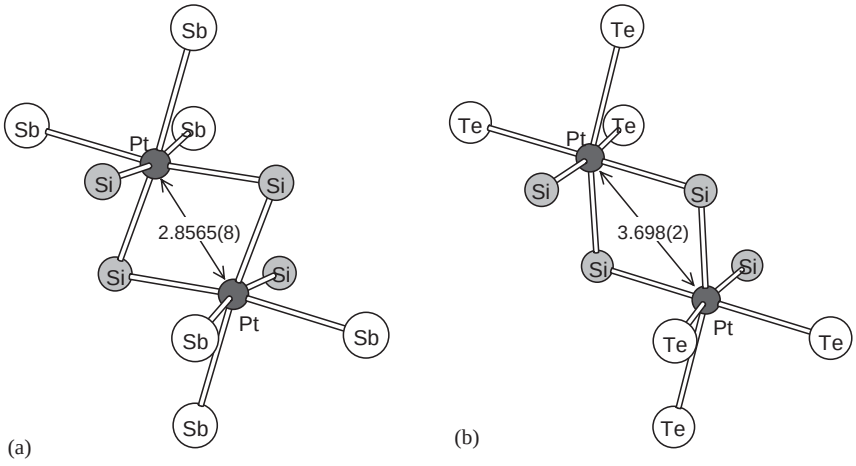

Fig. 2. Comparison of the edge-sharing octahedral dimers in (a) PtSiSb and (b) PtSiTe [9].

An important feature present in PtSiSb but not in α-$NiAs_2$ is the occurrence of metal–metal pairs. To quantify the distortion that ensues, the separation along *c* between the nets of metal atoms in the pyrite-type blocks can be compared with that in the marcasite-type blocks; effectively, this corresponds to the thickness of the blocks. Among the known α-$NiAs_2$-type compounds (CoAsSe [10], CoPSe [10], CoSbS [23], IrPTe [24], $NiAs_2$, $PtBi_2$ (originally classified less accurately as $AuSn_2$-type) [25], and PtSiTe [9]), the marcasite-type blocks are thicker than the pyrite-type blocks in all cases except CoSbS and PtSiTe. In the last two cases, the marcasite-type blocks are contracted to 2.8–2.9 Å thick owing to the placement of the smaller nonmetal atoms (S and Si, respectively) in these blocks, compared to the 3.0–3.3 Å thick pyrite-type blocks. In PtSiSb, the marcasite-type blocks are considerably contracted (2.448 Å) relative to the pyrite-type blocks (3.250 Å). Compared to PtSiTe, the distortion in PtSiSb is more than can be accounted for by mere size effects. Fig. 2 clearly shows that the Pt atoms within the edge-sharing octahedral dimer are displaced from the centers of the octahedra towards each other in PtSiSb but away from each other in PtSiTe, and the Pt–Pt separations differ by more than 0.8 Å!

3.2. Bonding

All known α-$NiAs_2$-type compounds have 20 valence electrons per formula unit. If the anion–anion pairs are assumed to be single bonds, applying the Zintl concept so that each nonmetal atom attains an octet leads to the conclusion that the transition-metal atoms have a d^6 configuration. For example, in PtSiTe, formal charges of Si^{3-} and Te^{1-} are assigned, implying a Pt^{4+} (d^6) oxidation state in this "conventional electron counting scheme" [16]. This assignment is also consistent with the 18-electron rule being fulfilled by the d^6 transition-metal centers, which are coordinated octahedrally by six ligands, each providing a lone pair of electrons. There is thus no need to form any metal–metal bond; consistent with this expectation, the metal–metal separation is greater than 3.3 Å in all α-$NiAs_2$-type compounds.

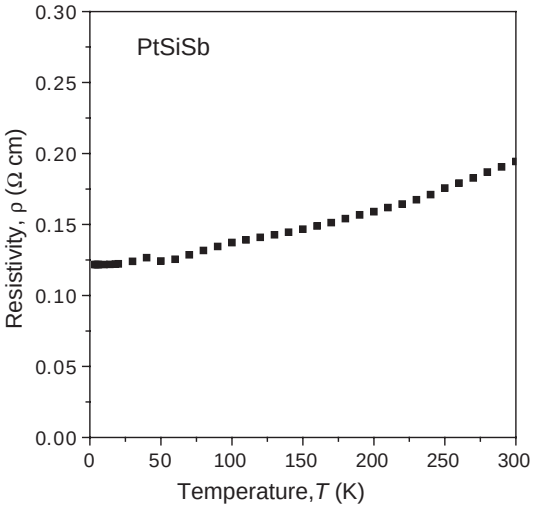

Fig. 3. Temperature dependence of the resistivity of PtSiSb.

In contrast, PtSiSb has 19 valence electrons per formula unit. The formulation $(Pt^{5+})(Si^{3-})(Sb^{2-})$ implies a d^5 configuration for the Pt centers. The 18-electron rule will then only be fulfilled if one Pt–Pt metal–metal bond is formed to each Pt atom, consistent with the observation of 2.8565(8) Å Pt–Pt pairs in the structure of PtSiSb. In this connection, the structure of PtSiSb is closely related to that of $AuSn_2$ (*Pbca*; *oP*24), which is also a 19-electron system. Although Au–Au pairs (2.98 Å) are present, no distinct anion–anion pairs occur, each Sn atom having two close Sn neighbors at 3.05 and 3.13 Å instead [26]. The closed-shell formulation $(Pt^{5+})(Si^{3-})(Sb^{2-})$ suggests that PtSiSb should be a normal valence compound possessing a band gap, likely small. Fig. 3 shows a representative plot of the

resistivity behavior for PtSiSb. The resistivity increases with temperature, but the dependence is too weak and the absolute values of the resistivity are too high for this behavior to be classified as metallic, although contact resistance may be a contribution that cannot be ruled out.

The problem with applying the electron counting scheme above is that Pt is not the least, but the most electronegative component in PtSiSb (Pauling electronegativities: Pt, 2.2; Si, 1.9; Sb, 2.0). However, full electron transfer from the nonmetal to the metal atoms to give a highly negative oxidation state on Pt would be unrealistic; this difficulty is similar to the situation in $PtSi_3P_2$ [16]. For compounds containing late transition metals and weakly electronegative nonmetals, a "modified electron counting scheme" has been recommended [16]. Accordingly, in the case of PtSiSb, the Pt atoms remain formally neutral with a d^{10} configuration.

The band structure of PtSiSb was calculated to examine the bonding and the influence of electron count in more detail. Fig. 4 shows the density of states (DOS) curve and its projections for the Pt 5*d*, Si 3*p*, and Sb 5*p* orbitals, and Fig. 5 shows the crystal orbital overlap population (COOP) curves for different contacts. The occurrence of a small band gap (0.6 eV) is consistent with the observed weak temperature dependence of the resistivity (Fig. 3) if real samples of PtSiSb are assumed to exhibit a small degree of nonstoichiometry or impurity doping levels to reach the exhaustion regime of a semiconductor. The Pt 5*d* states are nearly completely filled below the Fermi level, in a narrow region between −14 and −12 eV (Fig. 4a), supporting the assertion of a d^{10} configuration for Pt predicted by the modified electron counting scheme. Substantial mixing of the Pt, Si, and Sb states leads to optimization of strong Pt–Si, Pt–Sb, and Si–Sb covalent bonding, as verified by the occupation of all bonding and no

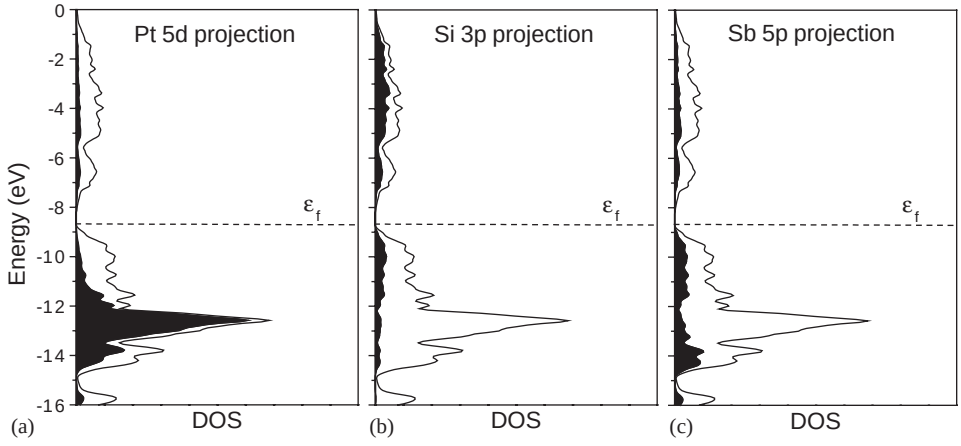

Fig. 4. Contributions of (a) Pt 5*d*, (b) Si 3*p*, and (c) Sb 5*p* orbitals (shaded regions) to the total DOS (line) for PtSiSb.

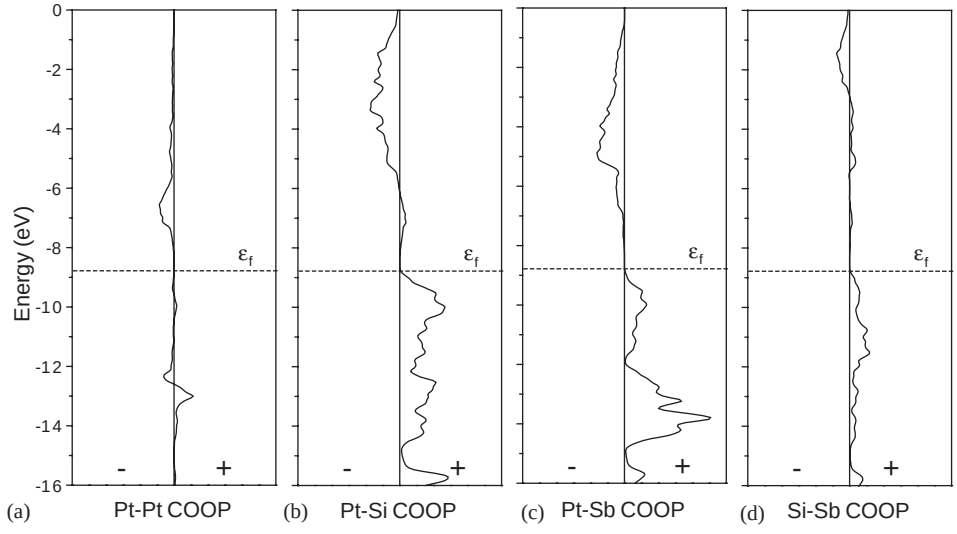

Fig. 5. COOP curves for (a) Pt–Pt, (b) Pt–Si, (c) Pt–Sb, (d) Si–Sb interactions in PtSiSb.

antibonding levels seen in the COOP curves (Fig. 5) and the large Mulliken overlap populations (MOP) listed in Table 3. Of particular interest is the significantly positive MOP of 0.093 for the 2.8565(8) Å Pt–Pt contact (cf., 0.097 for a 2.75 Å Pt–Pt distance in a model $Pt_2(PH_3)_4$ dimer [27]). Dispersion interactions between d^{10} cores probably provide the major component to Pt–Pt bonding. However, the contribution of covalent interactions arising from mixing of the 6*s* and 6*p* states cannot be discounted, so that there is net bonding despite the occupation of antibonding states (Fig. 5a). Analysis of the integrated atomic orbital projections indicates that the configuration of Pt is $5d^{9.2}\ 6s^{0.3}\ 6p^{1.2}$ in the compound.

If a rigid band model is assumed, adding an electron per formula unit to the system raises the Fermi level to –6.04 eV and forces more Pt–Pt antibonding levels to be occupied (Fig. 5a), thus providing a simple explanation for the disappearance of Pt–Pt bonding on going from PtSiSb to PtSiTe. An actual calculation on PtSiTe reveals, as expected, a similar band structure as PtSiSb but with a larger band gap (1.6 eV) because the atomic Te levels start off lower in energy. Table 3 lists the MOP values for various contacts in PtSiTe. The significantly negative MOP of −0.103 for the Pt–Pt contact confirms the absence of Pt–Pt bonding in PtSiTe.

In conclusion, PtSiSb represents an oxidized ($19e^-$) variant of PtSiTe and other α-$NiAs_2$-type structures ($20e^-$), accompanied by the formation of metal–metal bonded pairs involving a d^{10} configuration on Pt. This structural transformation is reminiscent of that between normal marcasites and arsenopyrites, for which a number of theoretical models have been proposed [28–32]. It would be interesting to study the evolution of metal–metal bonding on changing the electron count continuously, for example, in the solid solution $PtSiSb_{1-x}Te_x$. This has been attempted, but without success so far. Solid solutions based on other α-$NiAs_2$-type members may be worthwhile investigating.

Acknowledgments

The Natural Sciences and Engineering Research Council of Canada and the University of Alberta supported this work. We thank Dr. Robert McDonald (Faculty Service Officer, X-ray Crystallography Laboratory) for the X-ray data collection, Ms. Christina Barker (Department of Chemical and Materials Engineering) for assistance with the EDX analyses, and Mr. Devon Moore for assistance with the resistivity measurement.

References

[1] O.N. Il'nitskaya, Yu.B. Kuz'ma, V.S. Fundamenskii, Dopov. Akad. Nauk Ukr. RSR, Ser. A (1989) 79.
[2] O.N. Il'nitskaya, V.A. Bruskov, P.Yu. Zavalii, Yu.B. Kuz'ma, Izv. Akad. Nauk SSSR, Neorg. Mater. 27 (1991) 1311.
[3] O.N. Il'nitskaya, Yu.N. Grin', Yu.B. Kuz'ma, Kristallografiya 37 (1992) 146.
[4] J. Wallinda, W. Jeitschko, J. Solid State Chem. 114 (1995) 476.
[5] O.N. Il'nitskaya, P.Yu. Zavalii, Yu.B. Kuz'ma, Dopov. Akad. Nauk Ukr. RSR, Ser. B (1989) 38.
[6] S.V. Oryshchyn, V.S. Babizhets'ky, Yu.B. Kuz'ma, T. Głowiak, Z. Kristallogr. 214 (1999) 337.
[7] O.N. Il'nitskaya, Yu.B. Kuz'ma, Russ. J. Inorg. Chem. (Engl. Transl.) 35 (1990) 1104.
[8] Ch. Perrier, M. Kirschen, H. Vincent, U. Gottlieb, B. Chenevier, R. Madar, J. Solid State Chem. 113 (1997) 473.
[9] M.F. Mansuetto, J.A. Ibers, Z. Kristallogr. 209 (1994) 708.
[10] A. Kjekshus, T. Rakke, Acta Chem. Scand., Ser. A 33 (1979) 609.
[11] G.M. Sheldrick, SHELXTL, Version 5.10, Bruker AXS Inc., Madison, WI, 1998.
[12] A.J.C. Wilson (Ed.), International Tables for X-ray Crystallography, Vol. C, Kluwer, Dordrecht, 1992.
[13] L.M. Gelato, E. Parthé, J. Appl. Crystallogr. 20 (1987) 139.
[14] M.-H. Whangbo, R. Hoffmann, J. Am. Chem. Soc. 100 (1978) 6093.
[15] R. Hoffmann, Solids and Surfaces: A Chemist's View of Bonding in Extended Structures, VCH Publishers, New York, 1988.
[16] K.-S. Lee, H.-J. Koo, D. Dai, J. Ren, M.-H. Whangbo, Inorg. Chem. 38 (1999) 340.
[17] E.J. Graeber, R.J. Baughman, B. Morosin, Acta Crystallogr., Sect. B 29 (1973) 1991.
[18] N.E. Brese, H.G. von Schnering, Z. Anorg. Allg. Chem. 620 (1994) 393.
[19] J. Donohue, The Structures of the Elements, Wiley, New York, 1974.
[20] L. Pauling, The Nature of the Chemical Bond, 3rd Edition, Cornell University Press, Ithaca NY, 1960.
[21] W.N. Stassen, R.D. Heyding, Can. J. Chem. 46 (1968) 2159.
[22] M.E. Fleet, Am. Miner. 57 (1972) 1.
[23] J.F. Rowland, E.J. Gabe, S.R. Hall, Can. Miner. 13 (1975) 188.
[24] G. Kliche, Z. Naturforsch. B 41 (1986) 130.
[25] Y.C. Bhatt, K. Schubert, Z. Metallkde. 71 (1980) 581.
[26] K. Schubert, H. Breimer, R. Gohle, Z. Metallkde. 50 (1959) 146.
[27] A. Dedieu, R. Hoffmann, J. Am. Chem. Soc. 100 (1978) 2074.
[28] W.B. Pearson, Z. Kristallogr. 121 (1965) 449.
[29] J.B. Goodenough, J. Solid State Chem. 5 (1972) 144.
[30] J.A. Tossell, D.J. Vaughan, J.K. Burdett, Phys. Chem. Miner. 7 (1981) 177.
[31] J.K. Burdett, T.J. McLarnan, Inorg. Chem. 21 (1982) 1119.
[32] S.J. Wijeyesekera, R. Hoffmann, Inorg. Chem. 22 (1983) 3287.